Wireless Bioelectronics for In Vivo Pressure Monitoring with Mechanically-Compliant Hydrogel Biointerfaces

Jingsen Lin, Xingmei Chen, Pei Zhang, Yu Xue, Yinghui Feng, Zhipeng Ni, Yue Tao, Yafei Wang, and Ji Liu*

Recent electronics-tissues biointefacing technology has offered unprecedented opportunities for long-term disease diagnosis and treatment. It remains a grand challenge to robustly anchor the pressure sensing bioelectronics onto specific organs, since the periodically-varying stress generated by normal biological processes may pose high risk of interfacial failures. Here, a general yet reliable approach is reported to achieve the robust hydrogel interface between wireless pressure sensor and biological tissues/organs, featuring highly desirable mechanical compliance and swelling resistance, despite the direct contact with biofluids and dynamic conditions. The sensor is operated wirelessly through inductive coupling, characterizing minimal hysteresis, fast response times, excellent stability, and robustness, thus allowing for easy handling and eliminating the necessity for surgical extraction after a functional period. The operation of the wireless sensor has been demonstrated with a custom-made pressure sensing model and in vivo intracranial pressure monitoring in rats. This technology may be advantageous in real-time post-operative monitoring of various biological inner pressures after the reconstructive surgery, thus guaranteeing the timely treatment of lethal diseases.

1. Introduction

Implantable bioelectronics with capability to precisely and continuously sense critical physiological parameters, such as pressure, temperature, or bioelectrical signals within specific organs (i.e., brain, heart, lung, or bladder), are providing crucial diagnostic information for the treatment of a variety of chronic diseases.[1–7] Key enabling features are mechanically compliant components, which can form seamless integration between the bioelectronics and human skins, tissues, or even organs, thereby, the interfaces could provide soft mechanical coupling and efficient signal exchange, with mitigated tissue damage and inflammation response.[8–11] Although physical attachment has been widely used, such strategy is generally limited to epidermal bioelectronics, while not applicable to wet and dynamic biointerfaces, due to the intrinsically weak interactions (i.e., van der Waals interactions and/or capillary forces), as well as potential risk of detachment during the long-term applications.[4,12–15] Suturing has emerged as one of the most reliable routines to construct the electronics-tissue biointerfaces, however, it remains challenging for certain organs with intrinsic fragility or dynamic shape change and peristalsis (e.g., brain, heart, blood vessel, stomach, and bladder).[2,3,5,9,16,17]

Most recently, hydrogels show a great promise as an attractive class of biointerfacing materials, since they offer intrinsically chemical and structural similarity to biological tissues, enable functional and bidirectional interfaces, and also substantially alleviate the immune responses.[8,10,18] Although recent works on hydrogel bioadhesives have defined the routines for adhesion with various biological tissues, optimization of the hydrogel bioadhesives for implantable electronic biointerfacing that meet specific operational requirements and long-term robustness will likely lead to further opportunities and improvements in those key features.[19–23] Shortcomings of existing hydrogel bioadhesives, including weak interface, swelling-induced performance deterioration and complexity in handling the adhesives, have prevented them from providing conformal yet robust integration between bioelectronics and wet dynamic tissues/organs.[8,24] Especially, for pressure sensing bioelectronics, it is difficult to anchor these devices onto specific organs (i.e., brain, eyes, lungs, and bladders), since dynamic stress exerted by normal biological processes may lead to interfacial failures and air/fluid leaking.[9,25–27] Despite the clinical utilization of non-hydrogel-based bioadhesives, such as cyanoacrylate adhesives, the intrinsic high

J. Lin, X. Chen, P. Zhang, Y. Xue, Y. Feng, Z. Ni, Y. Tao, Y. Wang, J. Liu
Department of Mechanical and Energy Engineering
Southern University of Science and Technology
Shenzhen 518055, China
E-mail: liuj9@sustech.edu.cn

J. Liu
Shenzhen Key Laboratory of Intelligent Robotics and Flexible Manufacturing Systems
Southern University of Science and Technology
Shenzhen 518055, China

J. Liu
Guangdong Provincial Key Laboratory of Human-Augmentation and Rehabilitation Robotics in Universities
Southern University of Science and Technology
Shenzhen 518055, China

ADVANCED
SCIENCE NEWS

www.advancedsciencenews.com
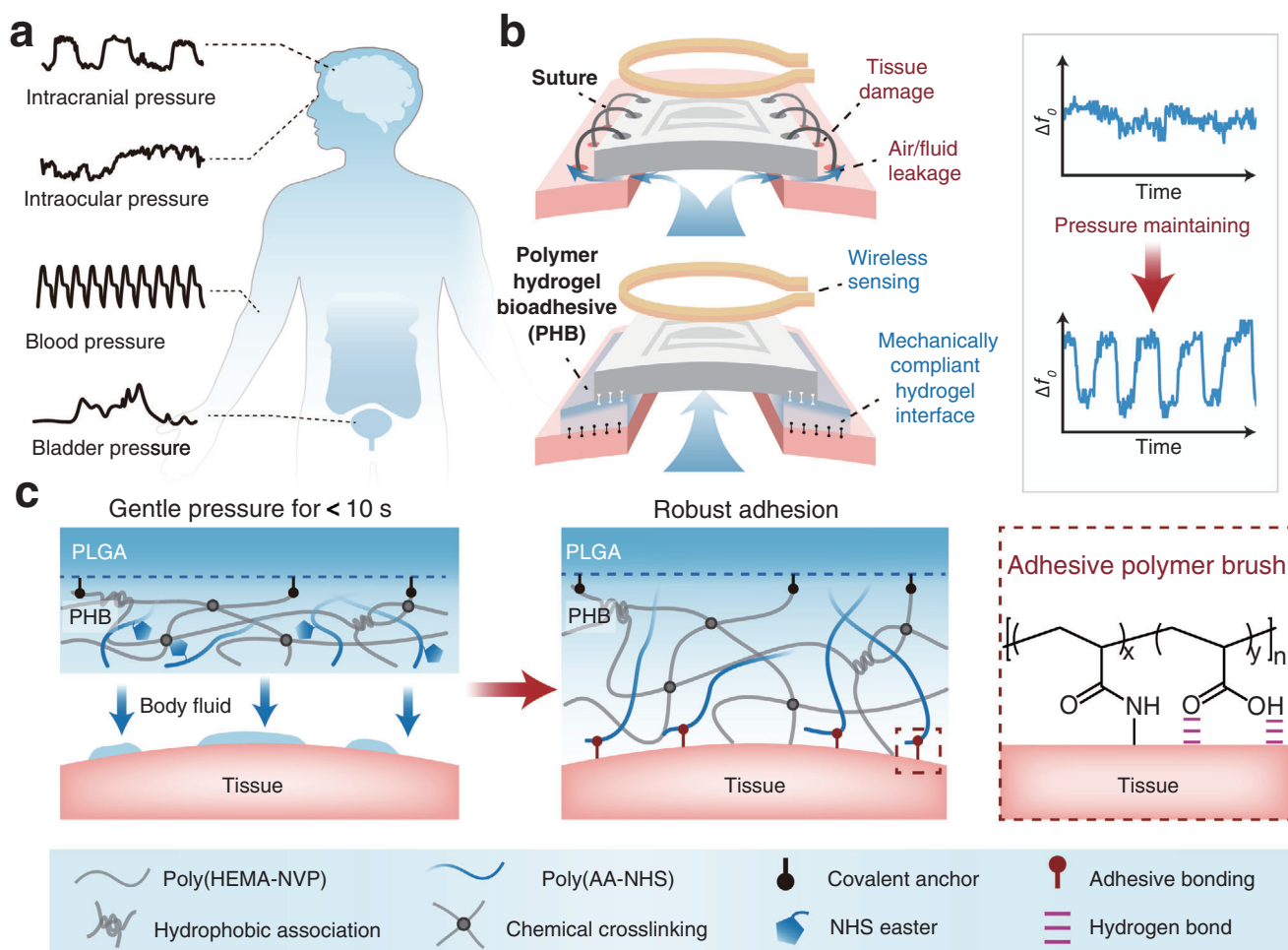
ADVANCED
MATERIALS

www.advmat.de

Figure 1. Design and fabrication of hydrogel biointerface for implantable pressure sensors anchorage. a) Schematic illustration of implantable bioelectronics for the in vivo biological pressure sensing within specific organs, such as brain, eyes, blood vessel, and bladder. b) Schematic illustrating the anchorage of wireless pressure sensor with a polymer hydrogel bioadhesive (PHB), change in pressure is captured wirelessly and passively with a readout coil adjacent to the implement site. Sharp difference in pressure signal is expected for the interface with or without robust hydrogel bioadhesion. For the sensor anchorage through suturing, inevitable gas/liquid leaking and tissue damage may deteriorate the reliability and lifespan of the in vivo pressure sensing. c) Schematic illustration of the PHB layer for establishing a robust biointerface between the wireless sensors and biological tissues. The hydrogel part of PHB dehydrates immediately upon contact with the biological tissues, and robust biointerface is built through the synergistic contribution from both amide bond formation (NHS moieties from PHB part and amine moieties from tissue part) and hydrogen bonding.

stiffness impedes natural movement of the elastic and soft tissues, thereby, considerable mechanical mismatch may result in tissue damage and/or device failures.[20,27] Bioelectronic interface, with capability to withstand a certain pressure for maintaining the inner fluid and/or air flow, has constituted a substantial barrier to the rapid innovation and broad application of implantable pressure sensors.[8,18]

Here, we report a general yet reliable approach to robustly anchor wireless pressure sensors onto the dynamical biological tissues/organs with a mechanically-compliant hydrogel biointerface (**Figure 1**). The hydrogel bioadhesives are composed of a sandwich structure, including a poly(HEMA-NVP) hydrogel substrate and adhesive poly(AA-NHS) polymer brushes. The instant and tough interfacial bioadhesion is constructed through the well-established dry cross-linking mechanism,[20,21] while swelling-resistant poly(HEMA-NVP) hydrogel substrate imparts the biointerface with long-term stability without performance

deterioration,[28] despite the direct contact with biofluids. Wireless operation is enabled by deploying the radio-frequency coupling strategy,[1,2] featuring a high sensitivity of 1 MHz mmHg^{-1} and sensing range of 0–40 mmHg. We have demonstrated the prospective utility of our hydrogel bioadhesives in forming a seamless bioelectronic-skull biointerface, allowing for the in vivo wireless and continuous intracranial pressure sensing in a rat model. This approach effectively mitigates the foreign body responses, but also addresses interfacial mechanical mismatch, thereby enhancing the efficacy of wireless pressure sensing. Furthermore, the wireless pressure sensing devices are entirely made of biodegradable materials, thus could be biodegraded and absorbed after several months, and eliminate the need for device removal. Our approach overcomes those key disadvantages of traditional electronics-tissues biointerfaces and may serve as the technical basis for the next-generation implantable bioelectronics.

**ADVANCED
SCIENCE NEWS**

www.advancedsciencenews.com

**ADVANCED
MATERIALS**

www.advmat.de

2. Results and Discussion

2.1. Fabrication of Hydrogel Bioadhesives

Thanks to the established biocompatibility and robust interfacial adhesion, hydrogel adhesives have been widely adopted as a versatile platform to anchor wearable and implantable devices onto the wet and dynamic tissues.[20,24,29] In our study here, we fabricated an adhesive hydrogel layer onto a poly(lactic-co-glycolic acid) (PLGA) substrate, which is widely used as a biocompatible and biodegradable encapsulation material for bioelectronics (Figure 1c).[12] A poly(2-hydroxyethyl methacrylate-co-N-vinylpyrrolidone) (poly(HEMA-NVP)) hydrogel layer was formed through radical copolymerization, while chemical anchorage of the poly(HEMA-NVP) chain onto an acrylate-functionalized PLGA substrate led to the PLGA/poly(HEMA-NVP) hybrid structure with robust interface (**Figure 2**a).[28] We then chemically grafted the adhesive polymer brushes, poly(acrylic acid-co-N-hydroxysuccinimide acrylate ester) (poly(AA-NHS)), onto the poly(HEMA-NVP) hydrogel substrate, resulting in our polymer hydrogel adhesives (PHB for abbreviation, Figure S1, Supporting Information). Optical microscopic image evidenced the distinct three-layer geometry of the PHB samples (Figure 2b), with the poly(AA-NHS) polymer chains penetrated within the poly(HEMA-NVP) hydrogel substrate (Figure S2, Supporting Information). Gradual decrease in both modulus and strength of the PHB/PLGA hybrid structure was detected during the three-step fabrication process (Figure 2c), thanks to the incorporation of hydrogel layer. The resulting PHB bioadhesive reached its equilibrium state after a 9-h immersion in PBS buffer (pH 7.4, 100 mM), maintaining a substantial water content of 80.2% (Figure 2d), with a tissue-like Young's modulus of ca. 100 kPa (Figures S3 and S4, Supporting Information). To achieve an instant and tough bioadhesion, our PHB hybrid structure adopted the well-established dry cross-linking mechanism, exploiting the synergetic contribution from non-covalent interactions (i.e., hydrogen bonding and electrostatic interactions) and covalent bonding between the NHS (hydrogel adhesive side) and amine moieties (tissue side).[20,21,28] Figure 2e and Movie S1 (Supporting Information) demonstrated that the adhered joint between the PHB and porcine skin can endure significant deformation, exhibiting a finger-like pattern before the initiation of interfacial crack propagation. Obviously, the PHB adhesive exhibited superior bioadhesion capability to porcine skin, with an interfacial toughness of 50 J m^{-2} and shear stress of 60 kPa. It is deserved to mention that the presence of a PLGA substrate did not notably affect the adhesive performance of the hydrogel adhesive layer (Figure S5, Supporting Information). The magnified microstructures corroborated the formation of conformal interface between the PHB and porcine tissue, thereby, resulting in a robustly adhered biointerface (Figure 2f).

To quantify the interfacial toughness and shear stress, we soaked the adhered joints within PBS buffer till equilibrium, followed by quantitative lap shear and peeling tests (Figure 2g; Figure S6, Supporting Information). The adhered interface exhibited a shear stress over 30 kPa even after 36-h soaking in PBS buffer. We reconstructed the adhesion interface in Abaqus (Figure S7, Supporting Information), with the PHB adhesives layer reaching its swelling-equilibrium state, and stress accumu-

lation was only detected within the circular area. Remarkably, upon application of the pressure, the interface separation remained below 0.0005 mm, indicating a completely bonded state. The resilient stability of the interface can be ascribed to the existence of phase segregation facilitated by hydrophobic association, coupled with inherent van der Waals interactions and hydrogen bonds.[30,31] The measured burst pressure for our PHB adhesives reached as high as 15 kPa (113 mmHg, Figure 2h; Figure S8, Supporting Information), surpassing that of previously reported hydrogel bioadhesives, such as GelMA.[32] Additionally, the burst pressure of the PHB bioadhesive significantly exceeded the critical value of physiological pressures, such as severe intracranial pressure (20−25 mmHg) and intraocular pressure (≈24 mmHg),[33,34] and such superior adhesion performance is particularly desirable for clinical pressure sensing. Different from the sandwiched structure (bioelectronics/hydrogel/biological tissues),[19–23] we elaborately integrated the hydrogel bioadhesives (poly(HEMA-NVP)/poly(AA-NHS)) with the PLGA substrate (commonly-used encapsulation material for implantable bioelectronics). Therefore, the PLGA/PHB hybrid could be readily used for various implantable bioelectronics, enabling the formation of a more robust biointerface than the sandwiched geometry (Figure S9, Supporting Information).

We also co-cultured the NIH3T3 cell line with our PHB samples to evaluate the in vitro biocompatibility and cell behaviors during culturing. No difference in quantitative cell viability (through CCK-8 assay) could be detected between the PHB bioadhesive samples (Figure 2i). We also observed a uniform monolayer of the NIH3T3 cells on the PHB substrate, featuring normal cell morphologies. Additionally, nearly no dead cells (red fluorescence) were observed upon live/dead cell staining, and the NIH3T3 cells substantially proliferated over tenfold within five days (Figure 2j).

2.2. Wireless Sensing

Currently, most implantable bioelectronics require wire connections and battery supplies, and these tethered solutions may cause undesirable discomforts and high risk of infection, tissue damage, and complications stemming from dislocation, leaking, and/or blocking.[8] Wireless bioelectronic devices, typically based on the inductor-capacitor (LC) circuits, possess the potential to circumvent these disadvantages.[2,10,17] Specifically, wireless sensors made of constituent materials, which can be decomposed into biologically benign end-products within the biofluids over a predesignated period, could effectively eliminate the devices after a functional period, thereby bypassing the need for surgical extraction.[6,12,21] In our study here, components used for the wireless devices were completely made of those commonly-used and biodegradable materials and could be easily processed, while a bench-top process involving laser cutting and physical lamination was adopted. The sensor assembly incorporated two 50-μm-thick Mg coils for the LC circuit, a 150-μm-thick PLGA film serving dual roles as the dielectric layer and packaging layer, a 100-μm-thick poly(1,8-octanediol-co-citrate) (POC) layer as the deformable support for the capacitor, and the PHB as the bioadhesive hydrogel interface (**Figure 3**a). Each constituent was meticulously designed in light of the biodegradability and

ADVANCED
SCIENCE NEWS
www.advancedsciencenews.com

ADVANCED
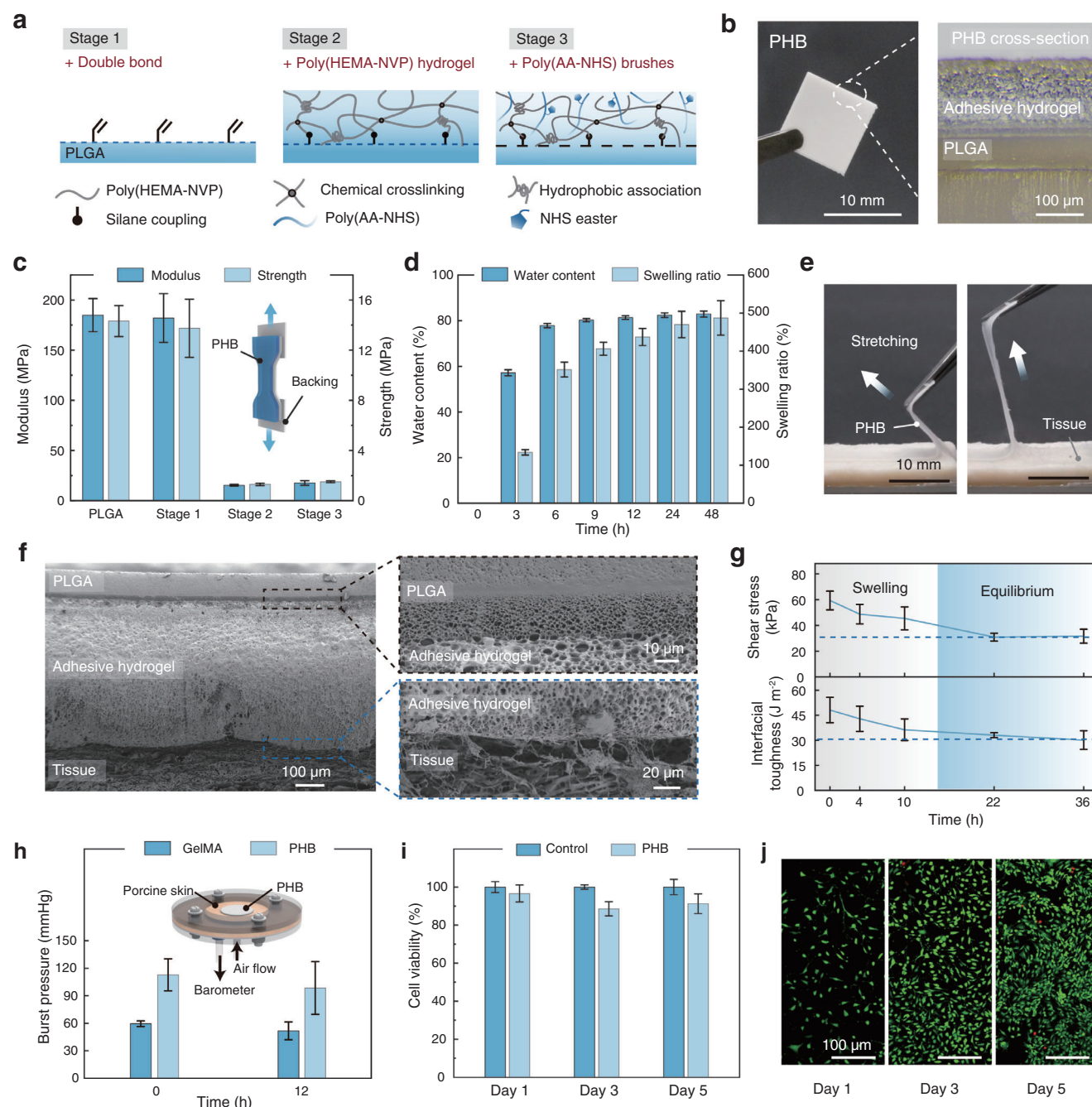**MATERIALS**
www.advmat.de

Figure 2. Structure characteristics and bioadhesion performance of the PHB. a) Schematic illustration of engineering the PLGA substrate with a polymer hydrogel bioadhesion (PHB) layer. The PLGA film was first functionalized with double bond, following by chemical grafting a conformal and swelling-resistant poly(HEMA-NVP) hydrogel layer. Subsequently, poly(AA-NHS) polymer brushes were introduced onto PLGA-poly(HEMA-NVP) hybrid structure, leading to the PHB structure. b) Images of PHB with a distinct three-layer structure. Scale bar: 10 mm (left); 100 μm (right). c) Evolution of the Young's modulus and strength of the PHB samples at different fabrication stages. A significant reduction in Young's modulus was observed during the transition from Stage 1 to Stage 2, attributed to the substantially high volume ratio of the hydrogel layer. d) Evolution of water content and swelling ratio of the PHB samples (dry state, 0 h) upon hydration within PBS buffer during 48 h. The equilibrium state is detected within 9 h. e) Images of peeling an adhered PHB sample from a porcine skin substrate. Structural deformation of the porcine skin corroborates the formation of a tough and mechanically conformal biointerface. Scale bar: 10 mm. f) SEM images of the adhered interface between the PHB and a biological tissue (porcine skin) upon lyophilization. Magnified image shows the distinct three-layer structure of the PHB, and also seamless and conformable interface between biological tissue and PHB. Scale bars are 100, 10, and 20 μm, respectively. g) Evolution of interfacial shear strength and toughness for the adhered joints between PHB and porcine skins, during the 36-h soaking within PBS buffer. h) Summary of the burst pressure of the PHB and GelMA for sealing a hole in porcine skin model, before and after soaking in PBS buffer for 12 h. The burst pressure of PHB samples is two times higher than that of severe intracranial hypertension (human, 40 mmHg), thus satisfying the purpose of intracranial pressure monitoring. i) Quantitative cell viability of NIH3T3 cells against the PHB samples after an incubation period of 1, 3, and 5 days. j) Representative fluorescent images of the NIH3T3 cells culturing on the surface of PHB samples, following the live (green) and dead (red) cell staining assay on Day 1, 3, and 5. Scale bar of 100 μm. Data in (c, d, g, h, i) are means ± S.D., $n = 3$.

**ADVANCED
SCIENCE NEWS**

www.advancedsciencenews.com

**ADVANCED
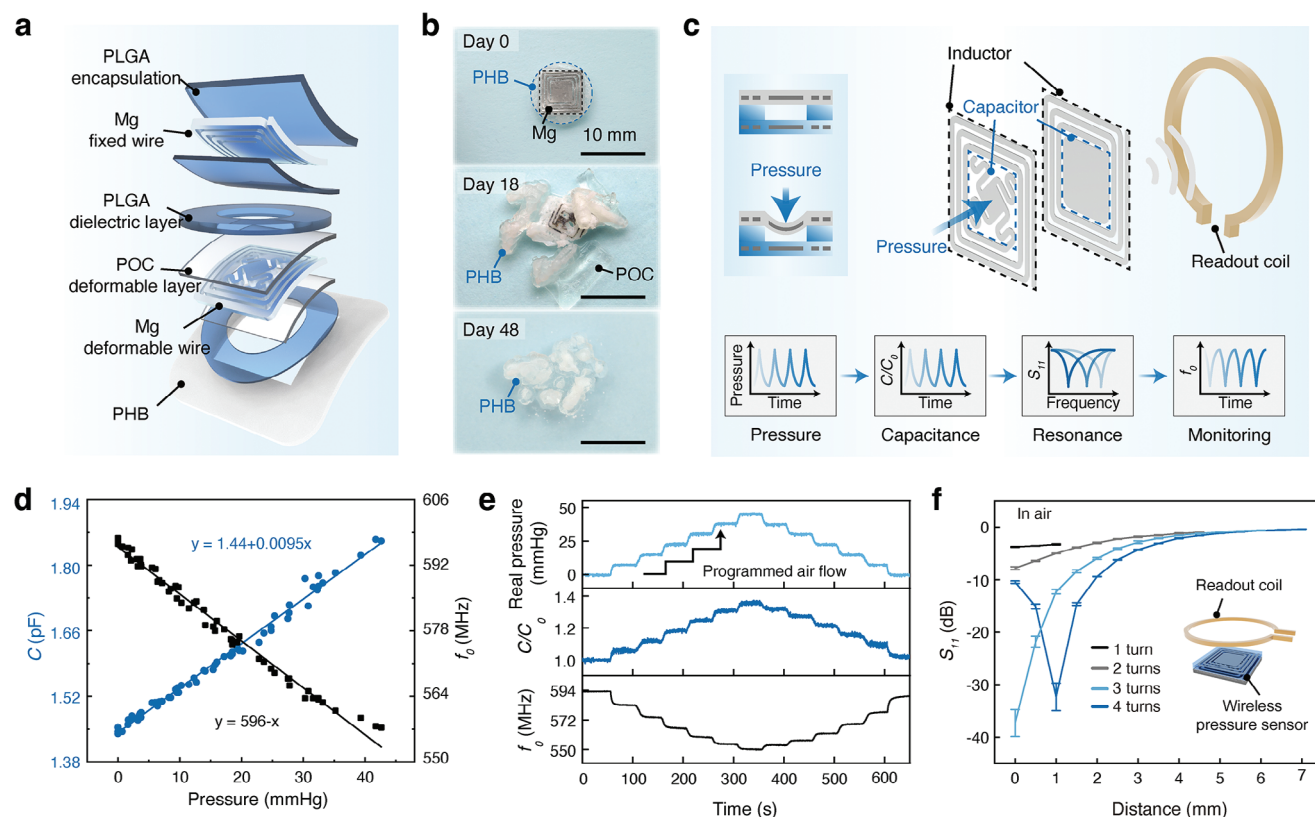MATERIALS**

www.advmat.de

Figure 3. Design and performance of the wireless pressure sensor. a) Exploded view of the fully-encapsulated wireless pressure sensor. The sensor is completely composed of biocompatibile and biodegradable materials, including Mg, PLGA, POC, and PHB. b) In vitro degradation of a wireless pressure sensor in PBS buffer with lipase from porcine pancreas at 37 °C on the Day 0, 18, and 48. Scale bar of 10 mm. c) Functional composition of the wireless sensor. The sensing function is enabled by the capacitor, which is composed of S-shaped and rectangle Mg plates. The outer double-layer coils constitute the inductor of the LC circuit, thus enabling the wireless signal sensing and transmission. The pressure of the fluid is sequentially converted into capacitance (C/C_0) and resonance frequency (f_0), which are simultaneously monitored through the readout coil. d) Capacitor and sensor response to an applied pressure within the range of 0 to 40 mmHg. Superior sensitivity is corroborated in this working range. e) Measured real pressure, C/C_0 and f_0 under stepwise pressure from 0 to 50 mmHg (50 s per step). The increase in pressure directly leads to the rise of C/C_0 and fall of f_0. f) Measured S_{11} of the wireless sensors with different number of coils at a sensing distance ranging from 0 to 7 mm in air. All data were measured at the same time. Data in (d, f) are means ± S.D., $n = 3$.

biocompatibility, alleviating concerns related to inflammation and the necessity for extraction through secondary surgery. Figure 3b illustrated the in vitro degradation process in a PBS/lipase buffer solution at 37 °C. The sensor progressively disintegrated, dissolved, and yielded small-sized fragments that persisted after a period of 48 days. While complete degradation may extend over a longer period, the material mass substantially diminished within the initial two weeks (Figures S10 and S11, Supporting Information). By elaborately tuning the thickness, size, and composition of the pressure sensor, the device's lifespan can be precisely regulated within any desired ranges. The complete LC circuits were formed by two overlapped yet separated laser-cut Mg coils (Figure S12, Supporting Information).[35] During the assembly, a crucial consideration was to ensure that the rotation direction of the two coils was consistent, and the circuits was precisely aligned, thereby, it could successfully prevent the significant baseline shifts of f_0 (resonant frequency of the LC circuit). This design intricately circumvented the need for intricate electrical connections, offering benefits in terms of process optimization and low-cost fabrication, as illustrated in Figure 3c.

The device was consisted of a parallel-plate capacitive sensor that was sensitive to any kinds of pressure, together with a bilayer coil structure for the wireless transmission of the radio-frequency data. Once the capacitor plate was deformed under external pressure, it was accompanied with a shift in resonant frequency ($f_0 = 1/\sqrt{(LC)}$) of the LC circuit. Real-time S_{11} spectrum was monitored wirelessly with a vector network analyzer (VNA) through a readout coil. Thereby, change in pressure can be wirelessly monitored through a battery-free approach (Figure 3c). The wireless pressure sensor was further simulated and analyzed through FEM analysis, integrating both the mechanical and electrostatic simulations. As shown in Figure S13 (Supporting Information), the shift of simulated f_0 upon compressing perfectly met our expectations for the in vivo physiological pressure monitoring.

The sensors were then characterized in a model that mimicked the change of in vivo physiological pressure (Figures S14–16, Supporting Information). Both the sensing capacitors and wireless pressure sensors were covered and sealed on a hole of a plastic box, which was equipped with an air pump and a barometer on each side (Movie S2, Supporting Information). The capacitors

**ADVANCED
SCIENCE NEWS**

www.advancedsciencenews.com

**ADVANCED
MATERIALS**

www.advmat.de

were connected to a LCR meter to measure the capacitance, while the readout coil was linked to a VNA for wireless measurement of the f_0. Remarkable sensitivity to the change in capacitance ($\approx$0.01 pF mmHg^{-1}) and f_0 (1 MHz mmHg^{-1}) was evidenced in Figure 3d. For even higher sensitivity, a larger size of the hole in dielectric layer could be used (Figure S16c, Supporting Information). To further mimic the practical detection of inner biological pressure, the capacitors and sensors were applied with stepwise pressure (Figure 3e). Both capacitance and f_0 were highly consistent with the applied pressure, showing great promise in real-time practical monitoring. With variation in the applied pressure, the sensing curves were characterized with accurate and prompt response with ignorable baseline shifting. Similar sensing performance was also detected with applied pressure with various frequencies and amplitudes (Figure S16d,e, Supporting Information). In our work here, wireless pressure sensors with various turns of coils were also fabricated, by taking into consideration the in vivo implant size and implantation depth for various application scenarios (Figure 3f; Figure S17, Supporting Information). Despite the attenuation of S_{11} intensity as the distance increased, the sensing performance could be improved significantly by increasing the turns of the coils. For example, by adding another one turn of coil, the S_{11} value of a four-turn device gained another 3.5-dB increase at a fixed sensing distance of 2 mm. As shown in the Figure S18a (Supporting Information), the simulation results was completely in consistence with the experimental curve in Figure 3f after subtracting the thickness of the encapsulation layer ($\approx$ 1 mm). The appearance of peak value might be associated with the decrease in mutual inductance, which was caused by the mismatch between the readout coil and the sensor (Figure S18b,c, Supporting Ifnformation).[27]

2.3. In Vitro Wireless Sensing Performance

By virtue of the significant differences in physical and chemical characteristics between electronic devices and biological tissues, deploying hydrogel bioadhesive to construct the seamless biointerface has emerged as the most promising strategy in current implantable bioelectronics. Our PHB adhesive was initially bonded onto a PLGA substrate, which is widely used as the encapsulation substrate, in light of its superior biocompatibility, biodegradability, and also flexibility. For the fabrication of wireless pressure sensor, the PLGA side was further exploited for device encapsulation, while the hydrogel side for bioadhesion. We then tested the in vitro wireless pressure sensing performance by assembling a model with porcine skins to mimic the internal biological pressures (**Figure 4a**), where robust interfacial sealing was perquisite. In the wireless sensing configuration, a sensor with three-turn coil and PHB (15 mm in diameter) layer was bonded onto a piece of porcine skin (a pre-cut hole of 4.5 mm in diameter) through the hydrogel adhesion. Another piece of porcine skin with a thickness of 1.5 mm was then laminated onto the pressure sensor (without interfacial adhesion), while the inner pressure was tuned by gradually purging air into the hole with an air pump. The readout coil, which was connected to a VNA, was put over the top of the porcine skin, allowing for the wireless and continuous pressure monitoring. Thanks to the robust hydrogel biointerface, the adhered joint between wireless sensor

and the porcine skin could sustain a dramatic structural deformation without interfacial failure (Figure 4b). It was also deserved to mention that no gas leaking was detected during the measurement, corroborating the robust interface constructed through our hydrogel bioadhesion technology.

The device was then placed within a simulated body fluid (PBS, pH = 7.4) to evaluate the signal attenuation (Figure 4c) with increased sensing distance. S_{11} reached $\approx$ -6.5 dB at a distance of 1.5 mm in PBS buffer, which was slightly larger than the corresponding value in air (Figure S19, Supporting Information). During the continuous pressure loading (Figure 4d), the measured f_0 remained constant at any fixed pressure and synchronously induced the changes in pressure, corroborating the robust adhesion interface with PHB and promise in long-term in vivo pressure monitoring. The device was characterized by simultaneously sensing the simulated pressure in vitro exerted by applied pulsed air with various frequencies and amplitudes (Figure 4e), demonstrating performances comparable to those commercially available pressure sensors. A high sensitivity of 1 MHz mmHg^{-1} and sensing range of 0–40 mmHg were quantified. In addition to the pulsed air purging, we also programmed the pressure in a stepwise manner (**Figure 4f**), and the synergistic change in f_0 corroborated the sensitivity of our wireless sensor.

2.4. In Vivo Intracranial Pressure (ICP) Monitoring

Continuous monitoring of inner pressures in those closed compartments of the human body, such as in the intracranial, blood vessel, and abdominal cavities, can provide crucial diagnostic and therapeutical information for various life-threatening diseases. For example, increase in intracranial pressure (ICP) by 5–10 mmHg after traumatic brain injuries results in ischemias where immediate medical intervention is indispensable.[36] Thereby, to avoid the un-timely treatment of lethal intracranial hypertension, it is necessary to conduct the continuous monitoring of the patients' ICP after craniocerebral surgery. Having established the robust biointerface between the wireless pressure sensor and biological tissues, as well as the biological decomposition of the pressure sensors and PHB layer, we further validated the potential for in vivo ICP monitoring with in a rat model (**Figure 5a**). A three-turn sensor with dimension of 6.4 mm (L) × 6.4 mm (W) was implanted over a burr hole drilled through the skull, which directly connected the cranial cavity and the pressure sensing devices (Figure 5b; Movie S3, Supporting Information). The interface between the ICP sensor and the skull tissue was build with the hydrogel biointerface through the dry crosslinking mechanism,[20] allowing for wireless measurements of ICP (Figure 5c). Some drift of the baseline occurred upon in vivo implantation (Figure S20, Supporting Information), which was likely due to transient flow of the interstitial and cerebrospinal fluids, accompanied with changes in the corresponding dielectric environment around the capacitor. Therefore, a re-calibration was indispensable for the in vivo wireless sensing (see Experimental Section for more details).

Squeezing the flank of the rat induced obvious changes in ICP across an expected range (Figure 5d; Figure S21, Supporting Information). This operation mimicked the increases in ICP due to intra-abdominal hypertension: compressing the
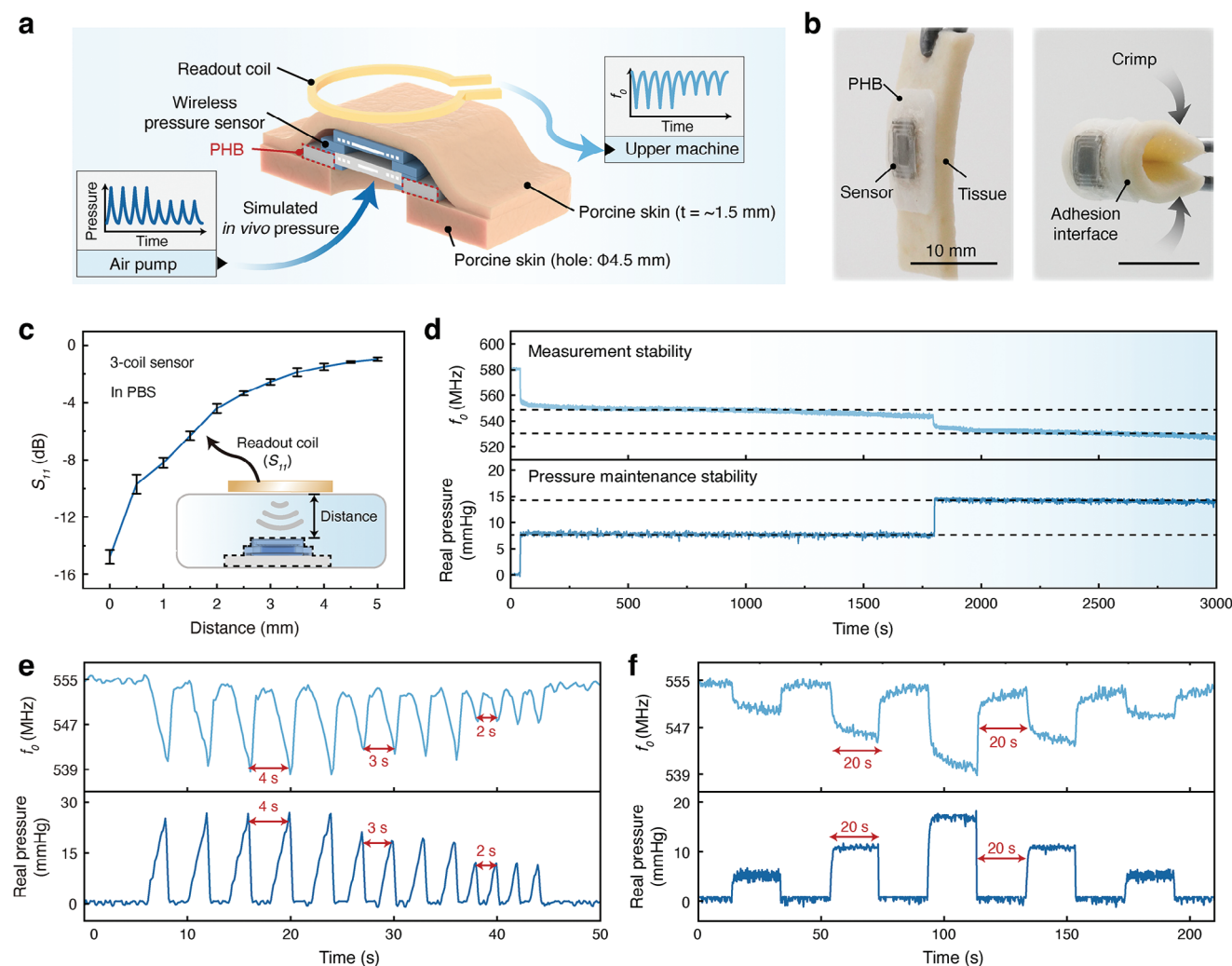
ADVANCED
SCIENCE NEWS

www.advancedsciencenews.com

ADVANCED
MATERIALS

www.advmat.de

Figure 4. Validation of wireless pressure sensing with PHB in a simulated environment. a) Schematic illustration of the set-up for in vitro experiment. The in vitro equipment mimics the wet environment under the skin, supplemented with a programmed air flow. After adhering the wireless pressure sensor to the hole (4.5 mm in diameter) and covered with a piece of porcine skin (1.5 mm in thickness), a readout coil connected to VNA is placed adjacent to the sensor for pressure monitoring. b) Images of the assembled sensor adhered onto a piece of biological tissue (i.e., porcine skin). The wireless pressure sensor could be robustly adhered onto the tissue under a large deformation (e.g., crimping). Scale bar: 10 mm. c) Wirelessly measured S_{11} of the pressure sensor within PBS buffer at a distance range from 0 to 5 mm using a 10-mm readout coil. d) Measured f_0 of the sensor under a continuous pressure loading for 3,000 s. The small deviation of f_0 corroborates the robust interface with PHB hydrogel bioadhesives and potential long-term in vivo pressure monitoring. e) Measured f_0 of the wireless pressure sensor under programmed pulse pressure. PHB offers a robust interface to maintain the inner pressure and prevent the potential air or fluid leaking. f) Measured f_0 of the sensor under stepwise pressure loading, featuring highly-desirable sensing robustness. Real pressure loaded is also monitored simultaneously and presented at the bottom of the chart in (d–f). Data in (c) are means ± S.D., $n = 3$.

abdominal cavity increased the intra-abdominal pressure, which in turn increased the ICP.[9] As demonstrated in Movie S4 (Supporting Information), upon squeezing and pressure releasing the flank of the rat, the VNA could track a significant shift in resonance point (f_0). This shift was highly synchronized with the applied pressure, thus played an important role in disease diagnosis, assessment and therapies. In contrast, without an adhesive interface, the sensor was incapable to detect any changes in ICP (Movie S5, Supporting Information). Meanwhile, the leakage of cranial contents would directly threaten lives of the rats. All these in vivo data demonstrated the crucial role of PHB adhesion to maintain inner pressure, which could

not be achieved with sutures or adhesive systems with weak interfaces.

Both the wireless sensor and hydrogel bioadhesive were fabricated with biodegradable materials, which could be decomposed into biologically benign end-products within the biofluids over a predesignated period of time; therefore, further surgical extraction could be effectively avoided. As per Micro-CT result, the Mg circuits within the device were predominantly decomposed on Day 14 (Figure 5e). A parallel degradation test was also conducted with the wireless sensor implanted subcutaneously with rats. On Day 21, remarkable millimetre-scale pores were detected on the surface due to the degradation of PLGA layer, with only fractional
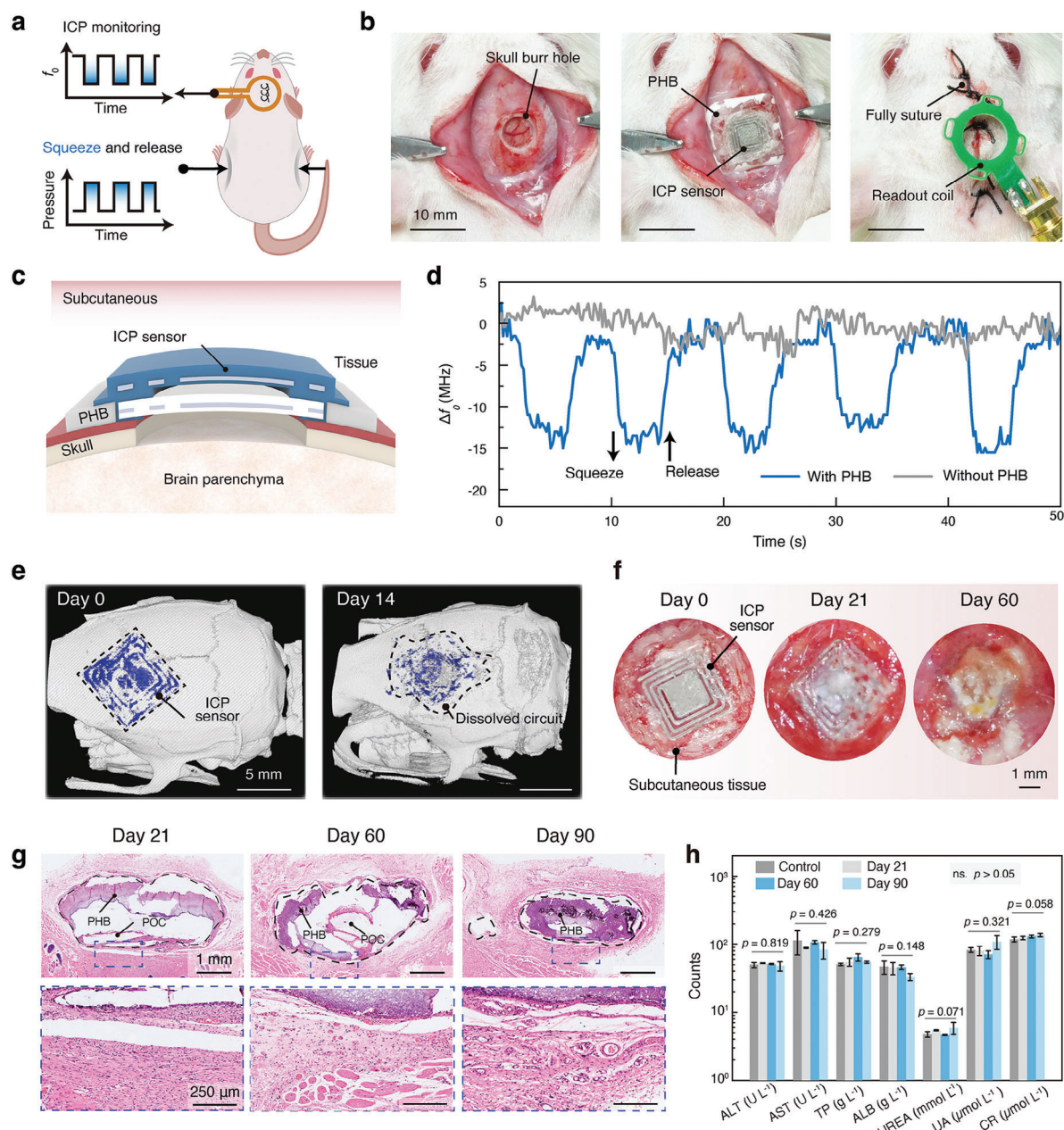
Figure 5. In vivo wireless monitoring of the intracranial pressure (ICP). a) Schematic illustration of the wireless in vivo measurement of the ICP. The flank of a rat is manually squeezed (5 s time^{-1}), in order to simulate the sharp changes in ICP. The capacitance of sensor increases and causes the decrease of f_0, which is simultaneously captured by VNA via a readout coil. b) The surgical operation of implanting a wireless pressure sensor for ICP measurement. The tissue on the surface of the skull was removed by a skin punch, and then a 5-mm diameter hole is created with an electric drill. After opening the dura, the wireless ICP sensor is quickly adhered to the tissue, allowing the sensor to directly contact with fluids in the intracranial space. Scale bar: 10 mm. c) Schematic illustration of the cross-section of the implanted ICP sensor with hydrogel biointerface. d) Measurements of f_0 while squeezing and releasing the flank of a rat. The rate of rise and fall of f_0 perfectly matches the frequency of squeezing and releasing the flank, evidencing the robust interface. e) Micro CT images of a three-turn ICP sensor subcutaneously implanted on the skull of a rat model at Day 0 and Day 14. The circuits of the sensor (marked in blue) became fragmented at Day 14, indicating the decomposition and adsorption of the constitute material (Mg). Scale bar: 5 mm. f) Images of the ICP sensors with PHB during the subcutaneous implantation at Day 0, 21, and 60. Compared to Day 0, the implanted sensor with PHB exhibits obvious signs of corrosion at Day 21, while the traces of the circuits are completely invisible at Day 60. Scale bar: 1 mm. g) Representative histological images stained with HE for the subcutaneously implanted wireless pressure sensor with PHB at 21, 60, and 90 days after implantation. Scale bar: 1 mm (top), 250 μm (bottom). h) Blood chemistry analysis of control (healthy animal without surgery) and animals with subcutaneously implanted wireless pressure sensor with PHB at 21, 60, and 90 days post-implantation. Liver function parameters include ALT (alanine transaminase), AST (aspartate transaminase), TP (total protein) and ALB (albumin). Renal function parameters include Urea, UA (uric acid), and CR (creatinine). Data in (h) are means ± S.D., $n = 3$. One-way analysis of variance (One-way ANOVA) is employed to determine the significance level between multiple groups, where $p > 0.05$ represents no significant difference.

**ADVANCED
SCIENCE NEWS**

www.advancedsciencenews.com

**ADVANCED
MATERIALS**

www.advmat.de

residues of the Mg circuits, while sensor circuit was completely decomposed on Day 60 (Figure 5f). Additionally, the degradation mechanism of PHB alone was also identified, showing that the PHB materials was decomposed into small fragments after 90 days (Figures S22 and S23, Supporting Information). The complete degradation of these components of the device is expected to occur over another several months. Histological evaluation of the implanted sensor showed a notable degradation and fragmentation after a 90-day implantation (Figure 5g; Figure S24, Supporting Information). To evaluate the potential systemic toxicity of the decomposed by-products, liver, and renal functional analyses were then conducted. Over a 90-day implantation, the liver and renal functions were comparable to those of healthy animals, indicating no marked signs of systematic toxicity (Figure 5h).

3. Conclusion

By creating a design strategy that synergistically combines the mechanically compliant hydrogel bioadhesion interface and the wireless sensing platform, we presented an implantable pressure sensor with highly desirable interfacial robustness, superior pressure sensitivity, fast response speed and repeatability, as well as in vivo biodegradability. Enabled by these properties, collectively, our wireless pressure device can continuously monitor the pressure change, which has also been demonstrated by quantitatively measuring the intracranial pressure in a rat model. Such hydrogel adhesives-based biointerfacing technology offers an effective routine for constructing tissue-bioelectronics interfaces, and also potentially be used for real-time physiological and clinical investigations in a next-generation personal health monitoring system.

4. Experimental Section

Preparation of the poly(HEMA-NVP)/poly(AA-NHS) Hydrogel Adhesives: The hydrogel adhesives were fabricated by chemically forming a thin poly(HEMA-NVP) hydrogel layer (0.72 mm in thickness) on a PLGA film (0.08 mm in thickness), followed by chemically growing another poly(AA-NHS) polymer brushes onto the poly(HEMA-NVP) hydrogel substrate. Briefly, the PLGA film was treated with oxygen plasma, then soaked into an ethanol/water solution (90/10 vol.%) of MSPMA silane, in order to anchor the methylacrylate moieties onto the PLGA substrate. The poly(HEMA-NVP) hydrogel layer was then formed through photopolymerization of HEMA/NVP precursor solution, and the PLGA/poly(HEMA-NVP) joints were formed through the chemical chain anchorage. After that, poly(AA-NHS) polymer brushes were chemically grafted into the poly(HEMA-NVP) hydrogel through the well-established protocol for surface initiated polymerization.[28] Finally, the as-formed hybrid sample was rinsed with acetic acid solution (2 wt%, Adamas) to remove excessive small molecules and free polymer chains, followed by air drying to yield a hybrid polymer film.

Assembly of the Wireless Sensors: The materials for the fabrication of biodegradable wireless pressure sensors were consisted of Mg, PLGA, POC, and PHB. Mg foil (50 μm) was cut into fixed and deformable wires according to the 3D models obtained form FEM simulation. Mg wires were soaked into ethanol/water solution (50/50 vol.%) and treated with an ultrasonic bath for 2 min, and then stored in a sealed container after air drying. The PLGA film (75:25, M_w = 87,000–106,000 Da) was prepared by solvent casting a PLGA/CH_2Cl_2 solution within a glass mould at room temperature. PLGA films of two different thicknesses, 150 and 30 μm, were fabricated by tuning the overall volume. The PLGA film with thickness of 150 μm was laser-cut into a ring shape and used as the dielectric layer to determine f_0 of the wireless pressure sensor under zero pressure, while the PLGA film with thickness of 30 μm was used as the packing materials to shape the Mg fixed wires. Each deformable coil was encapsulated with two pieces of low-modulus POC elastomer (100 μm). The fixed layer and deformable layer were separated by the dielectric layer and precisely aligned with each other. Finally, laser-cut PHB was seamlessly connected to the sensor by dissolving the PLGA layers with CH_2Cl_2. In order to completely evaporate the solvent, the fully assembled wireless sensor was placed within a ventilated condition for 12 h.

Wireless Pressure Sensing: Circuit of the test equipment was mainly consisted of a cavity, connected to a controllable pressure supplier and a measuring equipment (Figure S10, Supporting Information). The controllable pressure supply was realised by tuning the constant air flow with manual valve and electronic valve, which was controlled with a microcontrolle unit (Arduino UNO). By control the on/off periods of the electronic valve, the pressure with variable frequencies or amplitudes could be rationally tailored. Meanwhile, change of the pressure within the cavity was monitored in real time with a barometer (Krand, NP-15C030R). Changes in capacitance and f_0 could be continuously monitored with a LCR meter (Tonghui, TH2826) and benchtop VNA (Keysight, E5071C), respectively. The capacitance was recorded at a frequency of 100 kHz, and the data collected with VNA was further processed and analyzed with the software MATLAB.

The pressure supply for in vitro pressure sensing experiment was the same as the sensing test, as mentioned above. The only difference of the in vitro experiment was that the sensors were placed in a home-designed set to simulate the in vivo environment (Figure 4a). To evaluate the sensing capability, the purging pressure frequency and/or amplitude was rationally tuned, while change in f_0 was monitored with a VNA through the readout coil.

Experiments on Animal Subjects: All animal surgeries were reviewed and approved by the Committee on Animal Care at the Southern University of Science and Technology (Protocol Number: SUSTech-JY202201005). All biological porcine tissues and organs for ex vivo experiments were purchased from a meat production and processing company (Linyi Xincheng Jinluo Meat Products Group Co. LTD).

In Vivo Intracranial Pressure (ICP) Monitoring: SD rats (≈200–250 g) were first anaesthetised in a chamber (3 vol.% isoflurane in oxygen).[9,27] After the induction of anesthesia, the rat was transferred into a stereotaxic frame and maintained being anesthetized with a face mask (2 vol.% isoflurane in oxygen). A 2-cm incision on the skull was created to expose the thin tissue on skull. A craniectomy with 5-mm diameter on the head was made with an electric drill, and then a three-turn wireless ICP sensor was implanted on the skull. The PHB part was bonded onto the tissue under slight pressure (≈1 kPa) for 10 s, forming a tough adhesion interface and ensuring the sensor's capbility of monitoring. To induce a change in the ICP, the flank of the rat under anaesthesia was squeezed by hand for 5 s, and then the compression was unloaded for another for 5 s. The body temperature of the rat was kept at 40 °C with a heating pad. The change in f_0 was collected via a readout coil at a working distance of ≈2 mm.

Histological Analysis: Histological analysis was carried out to evaluate the inflammation response. Biological tissue samples collected from the animal models were fixed with 4 vol.% paraformaldehyde solution, dehydrated in sequence using gradient ethanol (75%–90%–95%–100%), and embedded in paraffin afterwards. The sample sectioning was conducted with a Leica RM2016 Cryostat (Leica, Germany) into slides of 4 μm in thickness, followed by hematoxylin and eosin (HE) and Masson trichrome staining. All the images were taken with an optical microscope (Pannoramic DESK, 3D HISTECH, Hungary).

Statistical Analysis: All results were presented as the mean ± standard deviation (S.D.). All experiments were repeated for at least three times and each condition was analyzed in triplicate. Data distribution was assumed to be normal for all parametric tests, two-sided t test and One-way analysis of variance (One-way ANOVA) were used to determine the significance level between two groups and multiple groups, respectively. The significance levels were considered as $p > 0.05$ represents no significant difference. All statistical analyzes were carried out with the Origin software package.

**ADVANCED
SCIENCE NEWS**

www.advancedsciencenews.com

**ADVANCED
MATERIALS**

www.advmat.de

Supporting Information

Supporting Information is available from the Wiley Online Library or from the author.

Acknowledgements

Conflict of Interest

The authors declare no conflict of interest.

Data Availability Statement

The data that support the findings of this study are available from the corresponding author upon reasonable request.

Keywords

[1] J. R. Sempionatto, J. A. Lasalde-Ramírez, K. Mahato, J. Wang, W. Gao, *Nat. Rev. Chem.* **2022**, *6*, 899.

[2] C. M. Boutry, L. Beker, Y. Kaizawa, C. Vassos, H. Tran, A. C. Hinckley, R. Pfattner, S. Niu, J. Li, J. Claverie, Z. Wang, J. Chang, P. M. Fox, Z. Bao, *Nat. Biomed. Eng.* **2019**, *3*, 47.

[3] D. H. Keum, S.-K. Kim, J. Koo, G.-H. Lee, C. Jeon, J. W. Mok, B. H. Mun, K. J. Lee, E. Kamrani, C.-K. Joo, S. Shin, J.-Y. Sim, D. Myung, S. H. Yun, Z. Bao, S. K. Hahn, *Sci. Adv.* **2020**, *6*, eaba3252.

[4] Y. Jiang, A. A. Trotsyuk, S. Niu, D. Henn, K. Chen, C.-C. Shih, M. R. Larson, A. M. Mermin-Bunnell, S. Mittal, J.-C. Lai, A. Saberi, E. Beard, S. Jing, D. Zhong, S. R. Steele, K. Sun, T. Jain, E. Zhao, C. R. Neimeth, W. G. Viana, J. Tang, D. Sivaraj, J. Padmanabhan, M. Rodrigues, D. P. Perrault, A. Chattopadhyay, Z. N. Maan, M. C. Leeolou, C. A. Bonham, S. H. Kwon, et al., *Nat. Biotech.* **2022**, *41*, 652.

[5] Y. Song, J. Min, Y. Yu, H. Wang, Y. Yang, H. Zhang, W. Gao, *Sci. Adv.* **2020**, *6*, eaay9842.

[6] M. Wang, Y. Yang, J. Min, Y. Song, J. Tu, D. Mukasa, C. Ye, C. Xu, N. Heflin, J. S. McCune, T. K. Hsiai, Z. Li, W. Gao, *Nat. Biomed. Eng.* **2022**, *6*, 1225.

[7] J. W. Kwak, M. Han, Z. Xie, H. U. Chung, J. Y. Lee, R. Avila, J. Yohay, X. Chen, C. Liang, M. Patel, I. Jung, J. Kim, M. Namkoong, K. Kwon, X. Guo, C. Ogle, D. Grande, D. Ryu, D. H. Kim, S. Madhvapathy, C. Liu, D. S. Yang, Y. Park, R. Caldwell, A. Banks, S. Xu, Y. Huang, S. Fatone, J. A. Rogers, *Sci. Transl. Med.* **2020**, *12*, eabc4327.

[8] R. Feiner, T. Dvir, *Nat. Rev. Mater.* **2017**, *3*, 1.

[9] J. Shin, Y. Yan, W. Bai, Y. Xue, P. Gamble, L. Tian, I. Kandela, C. R. Haney, W. Spees, Y. Lee, M. Choi, J. Ko, H. Ryu, J.-K. Chang, M. Pezhouh, S.-K. Kang, S. M. Won, K. J. Yu, J. Zhao, Y. K. Lee, M. R. MacEwan, S.-K. Song, Y. Huang, W. Z. Ray, J. A. Rogers, *Nat. Biomed. Eng.* **2019**, *3*, 37.

[10] C. Li, C. Guo, V. Fitzpatrick, A. Ibrahim, M. J. Zwierstra, P. Hanna, A. Lechtig, A. Nazarian, S. J. Lin, D. L. Kaplan, *Nat. Rev. Mater.* **2020**, *5*, 61.

[11] Y. Yu, J. Nassar, C. Xu, J. Min, Y. Yang, A. Dai, R. Doshi, A. Huang, Y. Song, R. Gehlhar, A. D. Ames, W. Gao, *Sci. Robot.* **2020**, *5*, eaaz7946.

[12] Y. Liu, J. Liu, S. Chen, T. Lei, Y. Kim, S. Niu, H. Wang, X. Wang, A. M. Foudeh, J. B.-H. Tok, Z. Bao, *Nat. Biomed. Eng.* **2019**, *3*, 58.

[13] P. Xu, S. Wang, A. Lin, H.-K. Min, Z. Zhou, W. Dou, Y. Sun, X. Huang, H. Tran, X. Liu, *Nat. Commun.* **2023**, *14*, 623.

[14] W. B. Han, G.-J. Ko, K.-G. Lee, D. Kim, J. H. Lee, S. M. Yang, D.-J. Kim, J.-W. Shin, T.-M. Jang, S. Han, H. Zhou, H. Kang, J. H. Lim, K. Rajaram, H. Cheng, Y.-D. Park, S. H. Kim, S.-W. Hwang, *Nat. Commun.* **2023**, *14*, 2263.

[15] V. R. Feig, H. Tran, M. Lee, Z. Bao, *Nat. Commun.* **2018**, *9*, 2740.

[16] S. Niu, N. Matsuhisa, L. Beker, J. Li, S. Wang, J. Wang, Y. Jiang, X. Yan, Y. Yun, W. Burnett, A. S. Y. Poon, J. B.-H. Tok, X. Chen, Z. Bao, *Nat. Electron.* **2019**, *2*, 361.

[17] K. Yamagishi, I. Kirino, I. Takahashi, H. Amano, S. Takeoka, Y. Morimoto, T. Fujie, *Nat. Biomed. Eng.* **2019**, *3*, 27.

[18] X. Liu, J. Liu, S. Lin, X. Zhao, *Mater. Today* **2020**, *36*, 102.

[19] J. Deng, H. Yuk, J. Wu, C. E. Varela, X. Chen, E. T. Roche, C. F. Guo, X. Zhao, *Nat. Mater.* **2021**, *20*, 229.

[20] K. Zhang, X. Chen, Y. Xue, J. Lin, X. Liang, J. Zhang, J. Zhang, G. Chen, C. Cai, J. Liu, *Adv. Funct. Mater.* **2022**, *32*, 2111465.

[21] Y. Xue, J. Zhang, X. Chen, J. Zhang, G. Chen, K. Zhang, J. Lin, C. Guo, J. Liu, *Adv. Funct. Mater.* **2021**, *31*, 2106446.

[22] Y. Xue, X. Chen, F. Wang, J. Lin, J. Liu, *Adv. Mater.* **2023**, *35*, 2304095.

[23] J. Zhang, L. Wang, Y. Xue, I. M. Lei, X. Chen, P. Zhang, C. Cai, X. Liang, Y. Lu, J. Liu, *Adv. Mater.* **2023**, *35*, 2209324.

[24] F. Wang, Y. Xue, X. Chen, P. Zhang, L. Shan, Q. Duan, J. Xing, Y. Lan, B. Lu, J. Liu, *Adv. Funct. Mater.* **2024**, 2314471, https://doi.org/10.1022/adfm.

[25] Z. Nie, J. W. Kwak, M. Han, J. A. Rogers, *Adv. Mater.* **2022**, https://doi.org/10.1002/adma.202205609.

[26] Q. Yang, S. Lee, Y. Xue, Y. Yan, T.-L. Liu, S.-K. Kang, Y. J. Lee, S. H. Lee, M.-H. Seo, D. Lu, J. Koo, M. R. MacEwan, R. T. Yin, W. Z. Ray, Y. Huang, J. A. Rogers, *Adv. Funct. Mater.* **2020**, *30*, 1910718.

[27] D. Lu, Y. Yan, Y. Deng, Q. Yang, J. Zhao, M.-H. Seo, W. Bai, M. R. MacEwan, Y. Huang, W. Z. Ray, J. A. Rogers, *Adv. Funct. Mater.* **2020**, *30*, 2003754.

[28] X. Chen, J. Zhang, G. Chen, Y. Xue, J. Zhang, X. Liang, I. M. Lei, J. Lin, B. B. Xu, J. Liu, *Adv. Funct. Mater.* **2022**, *32*, 2202285.

[29] Q. Yang, T. Wei, R. T. Yin, M. Wu, Y. Xu, J. Koo, Y. S. Choi, Z. Xie, S. W. Chen, I. Kandela, S. Yao, Y. Deng, R. Avila, T.-L. Liu, W. Bai, Y. Yang, M. Han, Q. Zhang, C. R. Haney, K. B. Lee, K. Aras, T. Wang, M.-H. Seo, H. Luan, S. M. Lee, A. Brikha, N. Ghoreishi-Haack, L. Tran, I. Stepien, F. Aird, et al., *Nat. Mater.* **2021**, *20*, 1559.

[30] F. J. Holly, M. F. Refojo, *J. Biomed. Mater. Res.* **1975**, *9*, 315.

[31] M. F. Refojo, *J. Polym. Sci. Polym. Chem.* **1967**, *5*, 3103.

[32] E. Shirzaei Sani, A. Kheirkhah, D. Rana, Z. Sun, W. Foulsham, A. Sheikhi, A. Khademhosseini, R. Dana, N. Annabi, *Sci. Adv.* **2019**, *5*, eaav1281.

[33] P. Le Roux, D. K. Menon, G. Citerio, P. Vespa, M. K. Bader, G. M. Brophy, M. N. Diringer, N. Stocchetti, W. Videtta, R. Armonda, N. Badjatia, J. Böesel, R. Chesnut, S. Chou, J. Claassen, M. Czosnyka, M. De Georgia, A. Figaji, J. Fugate, R. Helbok, D. Horowitz, P. Hutchinson, M. Kumar, M. McNett, C. Miller, A. Naidech, M. Oddo, D. Olson, K. O'Phelan, J. J. Provencio, et al., *Neurocrit. Care* **2014**, *21*, 1.

[34] M. O. Gordon, J. A. Beiser, J. D. Brandt, D. K. Heuer, E. J. Higginbotham, C. A. Johnson, J. L. Keltner, J. P. Miller, R. K. Parrish, M. R. Wilson, M. A. Kass, *Arch. Ophthalmol.* **2002**, *120*, 714.

[35] L. Y. Chen, B. C.-K. Tee, A. L. Chortos, G. Schwartz, V. Tse, D. J. Lipomi, H.-S. P. Wong, M. V. McConnell, Z. Bao, *Nat. Commun.* **2014**, *5*, 5028.

[36] S. Thompson, A. Coutts, C. Craven, A. Toma, L. Thorne, L. Watkins, *Acta Neurochir* **2017**, *159*, 485.